Received: 29 March 2020 | Revised: 15 June 2020 | Accepted: 16 June 2020

DOI: 10.1002/jbm.b.34678

Check for updates

Society For Biomaterials | WILEY

ORIGINAL RESEARCH REPORT

Microneedle-based transdermal electrochemical biosensors based on Prussian blue-gold nanohybrid modified screen-printed electrodes

Prem C. Pandey[1] | **Govind Pandey**[2] | **Roger J. Narayan**[3]

[1]Department of Chemistry, Indian Institute of Technology (BHU), Varanasi, India

[2]Department of Pediatrics, King George Medical College, Lucknow, India

[3]Joint Department of Biomedical Engineering, University of North Carolina and North Carolina State University, Raleigh, North Carolina

Correspondence
Prem C. Pandey, Department of Chemistry, Indian Institute of Technology (BHU), Varanasi, India.
Email: pcpandey.apc@iitbhu.ac.in

Funding information
Department of Science & Technology (India), Grant/Award Number: VJR-2017-000034

Abstract

We report on the fabrication of a microneedle-based electrochemical biosensor for use in transdermal biosensing, which includes a screen-printed electrode containing a Prussian blue-gold nanohybrid as the working electrode. The Prussian blue gold nanohybrid is made from polyethylenime (PEI)- mediated simultaneous synthesis of Prussian blue (PBNP) and gold nanoparticles (AuNP), which forms a PBNP-AuNP nanohybrid with a remarkable change in the Prussian blue character. PEI-protected polycrystalline PBNPs can be synthesized in acidic media from the single precursor potassium ferricyanide [$K_3Fe(CN)_6$] at 60°C. Since PEI also enables the controlled formation of gold nanoparticles (AuNPs) in the presence of formaldehyde, nanohybrids containing PBNPs and AuNPs may be prepared. Two different methods of PEI mediated synthesis of AuNP in the presence of PBNP were considered. In Method 1, AuNP and PBNP were made independently and mixed together in an appropriate ratio. In Method 2, PBNPs were made first, followed by PEI- and formaldehyde-mediated reduction of gold cations in the presence of PBNP. PBNP-AuNPs display a remarkable change in Prussian blue behavior such that the absorption maxima of PBNP-AuNPs made through Method 1 tend to increase at 670 nm as a function of gold concentration as compared with the control; the reverse was observed when PBNP-AuNPs were made through Method 2. As made PBNPs and PBNP-AuNPs made through Method 1 display excellent catalytic activity toward both reduction and oxidation of hydrogen peroxide based on peroxidase mimetic activity. In addition, the as-synthesized PBNPs displayed superparamagnetic behavior that can be manipulated in the presence of AuNPs. The results from peroxidase mimetic activity, chemiluminescence, cyclic voltammetry, and amperometry showed suitable analytical performance of the as-made PBNP-AuNP nanohybrid for biomedical applications.

KEYWORDS

amperometry, cyclic voltammetry, gold nanoparticles, peroxidase mimetic activity, polyethylenimine, Prussian blue nanoparticles

 © 2020 Wiley Periodicals LLC.

1 | INTRODUCTION

Microfabrication techniques such as additive manufacturing can be employed to create hollow microneedles for penetration of the top layers of the epidermal layer of the skin; these structures may be suitable for transdermal sensing of biologically-relevant chemicals (Gittard et al., 2009; Gittard et al., 2010; Gittard, Ovsianikov, Chichkov, Doraiswamy, & Narayan, 2010; Miller et al., 2016; Miller, Narayan, & Polsky, 2016; Skoog et al., 2015). For example, Miller et al. placed bundles of carbon fiber electrodes within the bores of digital micromirror device-based stereolithography-manufactured hollow acrylate-based polymer microneedles (Miller et al., 2011). The carbon fibers in these carbon fiber electrode-hollow microneedle devices were modified to enable detection of hydrogen peroxide. In another study, metallized carbon paste was loaded within the bores of hollow acrylate-based polymer microneedles; for example, metallized carbon paste was modified with lactate oxidase to enable detection of lactate (Windmiller et al., 2011). A microneedle array with multiple microcavities was integerated with a poly(o-phenylenediamine) thin film that was modified with glutamate oxidase and glucose oxidase (Windmiller et al., 2011). In another study, solid-state ion selective electrode for potassium ion detection was created out of a three-dimensional porous carbon (Miller et al., 2014). This electrode was integrated with a hollow microneedle; the functionality of the potassium ion selective electrode was shown over several concentration of potassium ions as well as in the presence of interfering sodium ions.

Microneedle-based sensors require precise positioning of the sensing components to yield an active sensing area in direct communication with the microneedle. Accordingly, microneedle-based sensors essentially require precise integration of the sensing electrode with microneedle array for reliable function. Such a requirement may be met out through screen-printing microfabrication technology, which provides structures with geometric features that exactly match the dimensions of the microneedle interface. The present report described the use of a suitably designed screen-printed electrode in which the Prussian blue gold nanoparticles nanohybrid is dispensed in controlled way for precise detection of hydrogen peroxide, an enzymatic reaction product of many oxidase enzyme-catalyzed reactions. As an example, the detection of a glucose oxidase-catalyzed reaction has also been examined in this study. The approach can be made even more practical with a portable electrochemical detector that is specifically designed for recognizing biologically-relevant chemical changes.

Structural, electronic, and magnetic evaluation of Prussian blue (PB) has revealed that Prussian blue and its analogs have potential applications in high-temperature molecular magnets, photo-switchable magnetic solids, antidotes for radioactive poisoning, molecular sieves, electrocatalytic materials, and hydrogen storage materials (Ding, Hu, Gu, & Xia, 2009; Entley & Girolami, 1995; Ferlay, Mallah, Ouahes, Veillet, & Verdaguer, 1995; Holmes & Girolami, 1999; Kaye & Long, 2005; Sato, Iyoda, Fujishima, & Hashimoto, 1996; Shatruk et al., 2007). To generate PB for these and other applications, it is necessary to develop a controlled synthesis protocol of PB given its inherent structural disorder (Windmiller, Zhou, et al., 2011). Furthermore, all Prussian blues are highly insoluble (Samain et al., 2013), with a solubility product of ca. 1×10^{-41}; as such, the preparation of water-soluble PB is of technological interest since water-soluble PB may be easier to integrate into future molecule-based electronic devices. Accordingly, attempts have been made to control Prussian blue nucleation, preventing the formation of an extended network and generating stabilized Prussian blue nanoparticles (PBNPs) (Pandey & Pandey, 2013a). Earlier studies demonstrated that the use of 3-aminopropyltrimethoxysilane (3-APTMS) along with cyclohexanone allow controlled conversion of PBNPs from the single precursor potassium ferricyanide [$K_3Fe(CN)_6$] with an average particle size on the order of 15.6 nm, justifying an electron transfer rate constant (32.1 s^{-1}) (Pandey & Panday, 2016; Pandey & Pandey, 2013a; Pandey & Pandey, 2013b; Pandey & Pandey, 2014). However, the PBNPs made with these reagents exhibited a poorly polycrystalline structure. It should be noted that a poorly polycrystalline structure of PB is associated with slower electrocatalytic activity. As such, an effort was made to maintain greater polycrystalline structure in the PB through a suitable reaction protocol that involved controlled conversion of a single precursor, $K_3Fe(CN)_6$, into PBNPs.

PB made from double precursors leads to the formation of crystalline PB, which exhibits limited solubility. The functionality of polyethylenimine (PEI), which enabled the conversion of double precursors into Prussian blue nanocubes, was recently demonstrated (Zhai, Zhai, Wang, & Dong, 2008). Polyethylenimine-protected Prussian Blue nanocubes, with an edge length of 50 nm and uniform size, were made from double precursors in an acidic medium containing PEI, $FeCl_3$, $K_3Fe(CN)_6$ and potassium chloride (Zhai et al., 2008). Since the use of double precursors is incompatible with electroanalytical applications, we synthesized water-soluble PBNPs using PEI from the single precursor $K_3Fe(CN)_6$. Indeed, synthesis of polycrystalline PBNPs with superparamagnetic behavior were demonstrated. As-made PBNPs have potential use for fabrication of PBNPs-modified electrodes with electrochemical activity for both electrochemical oxidation and reduction of H_2O_2.

In addition, as made PBNPs can function in homogeneous catalysis as peroxidase mimetics with catalytic ativity comparable to an enzyme. The catalytic activity of PB can be manipulated by incorporating AuNPs (Jing et al., 2014; Qiu, Peng, Liang, Li, & Xia, 2007). The synthesis of PB shell/Au core hybrid composites was carried out using double precursors; gold cations were reduced with trisodium citrate and tannic acid (Keihan, Karimi, & Sajjadi, 2020; Wang & Kan, 2018). These PB hybrid nanocomposites is not compatible with controlled dispensing over screen printed electrodes; this, a new protocol to make PB-Au nanocomposites is needed. The use of PEI for the conversion of potassium ferricyanide into PBNPs along with the reduction of gold cations is attractive; this approach may be explored to manipulate the catalytic activity of as-made peroxidase mimetic materials. The use of PEI for the reduction of gold cations into AuNPs through a thermal process has previously been demonstrated (Keihan et al., 2020; Sun, Dong, & Wang, 2004; Wang & Kan, 2018). Furthermore, we have recently demonstrated the role of PEI for controlled real time conversion of gold cations into gold nanoparticles (AuNPs) under ambient conditions in the presence of forrmaldehyde (Pandey, Pandey, & Narayan, 2017a; Pandey, Pandey, & Narayan, 2017b). Accordingly, nanohybrids of PBNPs and AuNPs can be made with PEI as a common reagent. The process of nanohybrid formation can be

controlled in two different ways. In Method 1, both PBNPs and AuNPs are made from PEI as the common reagent separately; these materials are then allowed to mix in an appropriate ratio. In Method 2, PBNPs are made first, followed by allowing the reduction of gold cations in the PBNP suspension in the presence of PEI and formaldehyde. The nanohybrids of PBNPs and AuNPs obtained from these two methods display remarkable change in Prussian blue character, as evidenced from transmission electron microscopy, ultraviolet–visible light spectroscopy, selected area electron diffraction, and electrochemical measurements. The results from peroxidase mimetic activity, cyclic voltammetry, and amperometry studies of the as-made PBNP-AuNP nanohybrids are considered in this study.

The luminol-H_2O_2 biointerface has been extensively explored in clinical diagnostics since hydrogen peroxide is one of the byproducts of an oxidase-catalyzed reaction. Peroxidase or its mimetic acts as potential catalyst for facilitating the chemiluminescence intensity of oxidized luminol, which is generated in the presence of the hydrogen peroxide during oxidase-enzyme catalyzed reactions. Accordingly, the luminol-H_2O_2 biointerface was used to evaluate the catalytic ability of a nanohybrid of PBNP-AuNPs based on the Scheme 1 reaction.

2 | EXPERIMENTAL PROCEDURE

2.1 | Materials

Potassium ferricyanide [$K_3Fe(CN)_6$] and hydrogen peroxide (H_2O_2) were purchased from Merck Limited (Mumbai, Maharashtra, India). Polyethylenimine (PEI) (MW. 60,000), Nujol mineral oil (density 0.838 g/ml), graphite powder (particle size 1–2 μm), and o-dianisidine were purchased from Sigma Aldrich Chemicals Pvt Ltd (Bengaluru, Karnataka, India). Tetrachloroauric acid ($HAuCl_4$) was purchased from HiMedia Laboratories (Mumbai, Maharashtra, India). All of the aqueous solutions were prepared using double distilled-deionized water from an Elga water purification system (High Wycombe, United Kingdom). All of the chemicals used in this study were of analytical grade with high purity. All of the experiments were performed at room temperature unless otherwise mentioned.

2.2 | Synthesis of cationic polymer coated PBNPs

The typical process of PBNPs synthesis involves mixing a 70 μl aqueous solution of $K_3Fe(CN)_6$ (0.05 M) and 20 μl of PEI (0.1 g/ml) using a vortex cyclomixer, followed by adding 5 μl of hydrochloric acid (HCl) (6.5 M). The resultant mixture was kept at 60°C in an oven for 3 hr. The yellow-colored solution turned deep blue as indicated by the absorption maximum recorded at 680 nm, indicating the formation of PBNPs. The optimum concentrations of $K_3Fe(CN)_6$ and PEI were achieved by varying the concentration of one component, while keeping the others fixed.

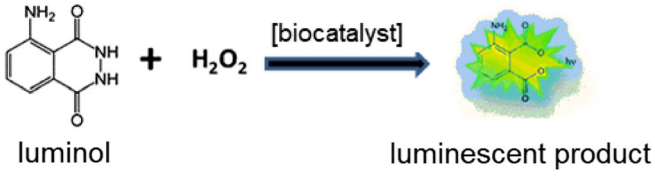

SCHEME 1 Chemiluminescence of the luminol-H_2O_2 biointerface in the presence of a biocatalyst

2.3 | Synthesis of PBNP-AuNP nanohybrids

The PEI-mediated formation of PBNPs was recorded at 60°C. AuNPs can be made from gold precursors in the presence of PEI and formaldehyde in less than 5 min at 25°C. Then, 25 mM of gold cations were mixed with 1 mg/ml of PEI in a methonic medium, followed by the addition of 20 μl of 40% formaldehyde under stirring conditions. The formation of AuNPs was initiated within 1 min after the addition of formaldehyde. The PBNP-AuNP nanohybrids were made using two different methods. In Method 1, AuNPs were made using three different concentrations of gold cations (100, 50, and 25 mM) using gold cation precursors (Pandey et al., 2017a). Equal volumes of PBNPs and AuNPs were thoroughly mixed to yield PBNP-AuNP nanohybrids. In Method 2, gold cations with three different concentrations (100, 50, and 25 mM) were treated with same amount of PEI (1 mg/ml). The as-made PEI-treated gold cations were mixed with same amount of PBNPs, followed by the addition of formaldehyde under stirring for 2–3 hr to yield the PBNP-AuNP nanohybrids.

2.4 | Materials characterization

All of the UV–VIS spectroscopy experiments were performed using a Hitachi U-2900 spectrophotometer (Tokyo, Japan). The X-ray diffraction (XRD) patterns were collected using a Rigaku Miniflex II diffractometer using CuKα (λ = 1.506 Å) radiation. The continuous mode was used for data collection over the 2θ range from 10° to 90°; a scanning speed of 4°/min was used in this study. Transmission electron microscopy (TEM) analysis was performed to ascertain particle size. TEM analysis of the as-synthesized PBNPs and AuNPs assembled PBNPs was performed using a JEOL JEM-2100F electron microscope (Tokyo, Japan), which was operated at 200 kV. To prepare samples for TEM analysis, a drop of the PBNPs or AuNPs assembled PBNPs solution was drop-cast onto a carbon-coated copper grid (mesh size-400) from Electron Microscopy Sciences (Hatfield, PA. The drop-cast carbon-coated copper grid was dried at room temperature and evaluated using TEM. The magnetic properties of the PB samples were measured on a magnetic property measurement system (MPMS®3) (Quantum Design Inc., MPMS-XL). The electrochemical measurements were performed with the CH Instruments 660B electrochemical workstation (Bee Cave, TX).

2.5 | Electrochemical measurements and preparation of the screen printed electrodes

Hollow microneedle arrays for electrochemical sensing were fabricated from three-dimensional drawings as described earlier (Miller et al., 2011; Windmiller, Zhou, et al., 2011). Three-dimensional

drawings were prepared using Magics software (Materialise NV, Leuven, Belgium). Additive manufacturing of the microneedle array was performed using a Perfactory III SXGA+ system (EnvisionTEC GmbH, Gladbeck, Germany), which contains a 150-W halogen bulb light source. A Digital Micromirror Device (DMD) SXGA+ guidance chip with 1,280 × 1,024-pixel resolution was used for selective polymerization of a liquid e-Shell 200 resin. The microneedle array was then washed in isopropanol to remove unpolymerized polymer. Post-building curing of the microneedle array was accomplished using an Otoflash Post Curing System instrument (EnvisionTEC GmbH, Gladbeck, Germany), which emits light over a wavelength range of 300–700 nm.

The typical process for the fabrication of the screen printed electrodes involved the use of five stencils made of polyester or steel with mesh size 160/375 in a three electrode configuration that matched the design of the microneedle array. An indigenous screen printer was used for screen printing the conducting inks. The silver, graphite, and Ag/AgCl conducting inks were printed using the stencils fixed in a semiautomatic screen printer using the squeeze and flood bar at an appropriate pressure, with complete alignment of printing exposure. The result of the screen printing step was screen printed electrode that contained a graphite working electrode, a graphite counter electrode and an Ag/AgCl reference electrode (Scheme 2). The PEI-protected PB nanoparticle colloidal suspension was dispensed over the working portion of the screen printed electrode directly after fabrication and cured at 110°C prior to use. The microneedle was fixed in place with an epoxy resin.

The electrochemical measurements were undertaken with a CHI 660B electrochemical workstation in a three-electrode configuration; a working solution of 3 ml was used in this study. The working electrode was PBNPs-modified graphite paste electrodes or AuNPs-assembled PBNPs modified graphite paste electrodes. Platinum foil and Ag/AgCl electrode served as the counter and reference electrode, respectively. Cyclic voltammetry at various scan rates from 0.01 to 0.3 V/s was performed at the graphite paste modified electrode; the dependency of scan rate (ν) on the peak current density (j) was analyzed. Electrochemical oxidation and reduction of H_2O_2 were performed in 0.1 M phosphate buffer containing 0.5 M KCl as the supporting electrolyte.

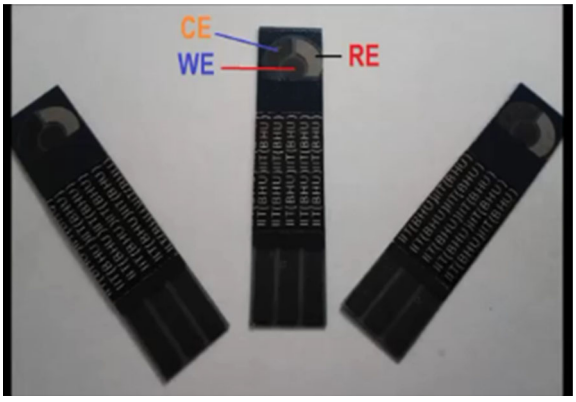

SCHEME 2 Electrodes made by screen printing

The modified electrode was created by adsorption of PBNPs solution or AuNPs assembled PBNPs solution onto the graphite powder (1–2 μm); the mixture was then dried at 60°C overnight. The active paste contained the following components: PBNPs and AuNPs-PBNPs 2.5% (wt/wt), graphite powder 67.5% (wt/wt), and Nujol mineral oil 30% (wt/wt). The well of the electrode body (MF-2010), which was obtained from Bioanalytical Systems (West Lafayette, IN) was filled with active graphite paste; the electrode paste surface was manually smoothed on a clean paper.

2.6 | Glucose oxidase catalyzed sensing of glucose

The use of PBNP-AuNp nanohybrids for probing the glucose oxidase-catalyzed reaction was evaluated. The modified electrode was made by mixing 2.5% PBNPs or AuNPs-PBNPs (wt/wt), 62% graphite powder (1–2 μm) (wt/wt), 5.5% glucose oxidase, and 30% Nujol mineral oil (wt/wt); the mixture was dried at 60°C overnight. The well of the MF-2010 electrode body (Bioanalytical Systems, West Lafayette, IN) was filled with active graphite paste; the electrode paste surface was manually smoothed on a clean paper.

2.7 | Peroxidase-like activity of PBNPs and AuNPs assembled PBNPs

The peroxidase-like activity of PBNPs and AuNPs assembled PBNPs was determined as described in other studies (Pandey & Panday, 2016; Pandey & Pandey, 2013b). In a typical situation, the peroxidase-like activity of as-synthesized PBNPs and AuNPs assembled PBNPs was determined spectrophotometrically by measuring the synthesis of the oxidized product of o-dianisidine at 430 nm (ε = 11.3 mM/cm) using a Hitachi U-2900 spectrophotometer as described earlier (Ferlay et al., 1995). The formation of the oxidized product of o-dianisidine, which is brown in color, in 0.1 M phosphate buffer (pH 7.0) in the presence of a varying concentration of H_2O_2 (0–25 mM) and 50 μM o-dianisidine was examined; measurements were obtained at 25°C using a constant concentration of PBNPs.

The steady-state kinetics study has previously been described in detail (Pandey & Panday, 2016). Briefly, steady-state kinetics was performed by varying the H_2O_2 concentration (0–25 mM) at a fixed concentration of o-dianisidine (50 μM). Each reaction was performed in 2 ml phosphate buffer (0.1 M, pH = 7). The variation of absorbance was measured as a function of time at a fixed wavelength of 430 nm (ε = 11.3 mM/cm). The Michaelis–Menten equation was used to calculate the kinetic parameters by fitting the absorbance data according to:

$$V = V_{max}[C]/K_m + [C] \quad (1)$$

In this equation, V represents the rate of conversion, V_{max} is the maximal reaction velocity, C is the concentration of the substrate, and K_m is the Michaelis-Menton constant.

The luminol-H_2O_2 system was used for chemical characterization of the biointerface generated in the presence of glucose oxidase and glucose based on chemiluminescent measurements that were catalyzed by the PBNP/PBNP-AuNP nanohybrids. The glucose oxidation experiment was performed in centrifuge tubes using 500 mg/dl glucose, keeping the amount of glucose oxidase fixed at 200 U/ml. The reaction was allowed to occur for at most 5–10 min. Then, 50 µl of the reaction product was mixed with 50 µl of luminol, followed by the addition of PBNPs or nanohybrids of PBNP-AuNP in a 2 ml fluorescence cuvette. The chemiluminescence was monitored using a F-7000 Hitachi fluorescence spectrophotometer (Tokyo, Japan).

3 | RESULTS AND DISCUSSION

3.1 | PEI mediated synthesis of PBNPs

At first, attempts were made to understand the process of PEI-mediated conversion of $K_3Fe(CN)_6$ into PBNPs. The results demonstrated that PEI enabled the conversion of $K_3Fe(CN)_6$ into PBNPs at 60°C within 3 hr. The results shown in Figure 1a,b demonstrate the role of each component, $K_3Fe(CN)_6$ and PEI, during the proposed reaction protocol for PBNPs synthesis. The composition of each reaction component, $K_3Fe(CN)_6$ and PEI, plays an important role in this type of conversion. The optimum concentrations of $K_3Fe(CN)_6$ and PEI (as evaluated from the absorbance recorded at 680 nm) were achieved by varying the concentration of one component while keeping a fixed concentration of the other component (Figure 1a,b). When all of the components are present in optimum concentrations, the conversion of single precursors into stable, well-dispersed, polycrystalline PBNPs (Figure 1c, Image III) at 60°C in 3 hr is enabled. However, the absence of either component does not lead to the synthesis of PBNPs (Figure 1c,I) and (Figure 1c,II).

Polyethylenimine (PEI) in an acidic medium precisely controls the nucleation of Prussian blue nanoparticles from $K_3Fe(CN)_6$, followed by conversion of the PEI to a positively charged polymer (Figure 2a; Scheme 1). The approach is similar to the one previously described for PEI-mediated reduction of gold cations (Keihan et al., 2020; Wang & Kan, 2018). The negatively charged centers of Prussian blue (PB) facilitate electrostatic interactions with cationic polymer centers, resulting in a cationic polymer coating that enables the formation of nanoparticles. Under similar conditions, the exchange of $K_3[Fe(CN)_6]$ with the gold salt ($HAuCl_4$) yields the formation of AuNPs (Figure 2b). When the formation of AuNPs is allowed to take place in a solution containing as-made PBNPs, self-assembly of AuNPs on a polycationic surface is observed (Figure 2c); a several-fold enhancement in the catalytic behavior of the material is noted. The process of PEI-mediated synthesis of PBNPs may proceed along the following steps: (a) in an acidic medium, some ferricyanide ions slowly and partially dissociate, leading to the formation of some undissociated ferricyanide ions and some Fe^{2+} ions; (b) in the presence of PEI, which acts as a reducing agent and a stabilizing agent, Fe^{3+} ions are reduced to Fe^{2+} ions; (c) undissociated ferricyanide ions and as-generated Fe^{2+} ions react, leading to the synthesis of PBNPs (Scheme 3).

3.2 | Formation of PBNP-AuNP Nanohybrids

PEI enables controlled conversion of gold cations into AuNPs in the presence of formaldehyde and other similar agents as described previously (Pandey et al., 2017a; Pandey et al., 2017b). Accordingly, PEI protected PBNPs can be used for making PBNP-AuNP nanohybrids. Two different approaches were used to make PBNP-AuNP nanohybrids. In Method 1, PBNPs and AuNPs are made separately and mixed together in an appropriate ratio. In this case, AuNPs were made from various concentrations of gold cation precursors (100, 50,

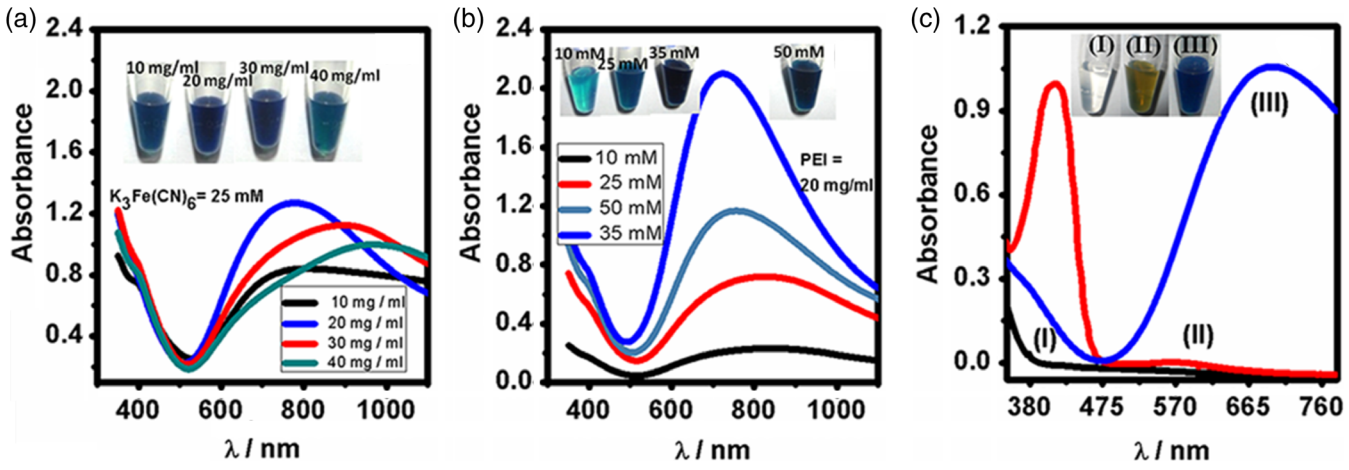

FIGURE 1 UV–Vis spectra of (a) a system containing a constant concentration of potassium ferricyanide (25 mM) and various concentrations of PEI (from 10 to 40 mg/ml); (b) a system containing a constant concentration of PEI (20 mg/ml) and various concentrations of potassium ferricyanide (from 10 to 50 mM); and (c) absorbance of only PEI (I), potassium ferricyanide (II), and PBNP (III) made from 20 mg/ml PEI and 35 mM potassium ferricyanide

and 25 mM); these AuNPs were used to make PBNP-AuNPs. In Method 2, PEI treated gold cations were reduced in the presence of PBNPs and formaldehyde. Three concentrations of gold cation precursors were studied (e.g., 100, 50, and 25 mM) using Method 2. The formation of PBNP-AuNP nanohybrids made from these methods were evaluated from UV–VIS spectroscopy (Figure 3). Figure 3a shows the

$$K_3[Fe(CN)_6] \xrightarrow{HCl} [Fe(CN)_6]^{3-} + Fe^{3+} \quad (1)$$

Potassium ferricyanide

$$Fe^{3+} \xrightarrow[60^\circ C,\ 3\ Hours]{Polyethylenimine} Fe^{2+} \quad (2)$$

$$[Fe(CN)_6]^{3-} + Fe^{2+} \xrightarrow[60^\circ C,\ 3\ Hours]{HCl,\ Polyethylenimine} Fe_4[Fe(CN)_6]_3 \quad (3)$$

Prussian blue

SCHEME 3 Scheme for polyethylenimine-mediated synthesis of PBNPs

UV–VIS spectra of PBNP-AuNP nanohybrids made through Method 1 from three different concentrations of gold cation precursors. Absorbance data at 670 nm from PBNP-AuNP nanohybrids was compared with absorption data at 670 nm from PBNPs in absence of AuNPs. The results show an increase in absorbance at 670 nm after the addition of AuNPs. The effect of gold cation precursor concentration on nanohybrid absorbance was examined (Figure 3a, i, ii, and iii); the absorption increased 0.6 to 1.2 for an increase in the gold cation precursor concentration from 25 to 50 mM; there was a small decrease in absorbance for a gold cation precursor concentration of 100 mM. PBNP-AuNPs made through Method 2 showed the opposite relationship for an increase in the concentration of gold cation precursors; the absorption decreased with an increase in the gold cation concentration from 25 to 100 mM as shown in Figure 3b, i, ii, iii. These results indicate that the PBNP character as determined from PBNP absorption at 670 nm is highly susceptible to the mode of PBNP-AuNP interactions.

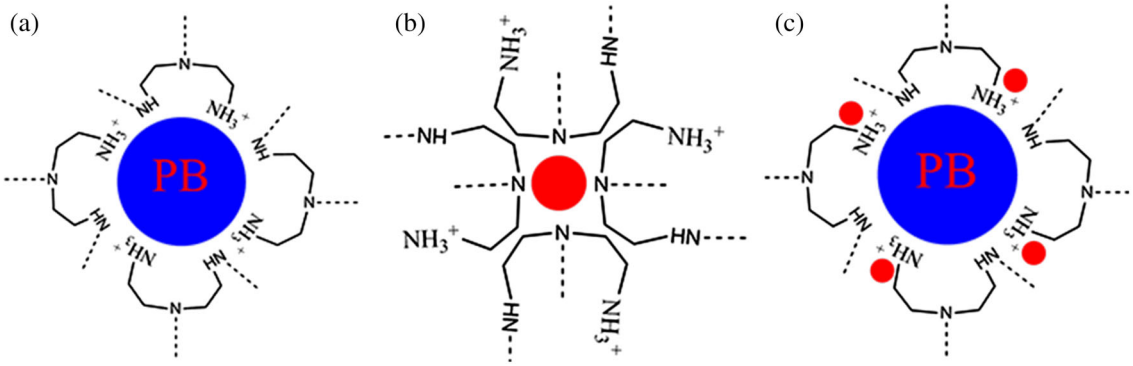

FIGURE 2 Schematic presentation of cationic polymer coating and formation of (a) PBNPs, (b) AuNPs, and (c) AuNPs assembled on cationic surface of PBNPs (c)

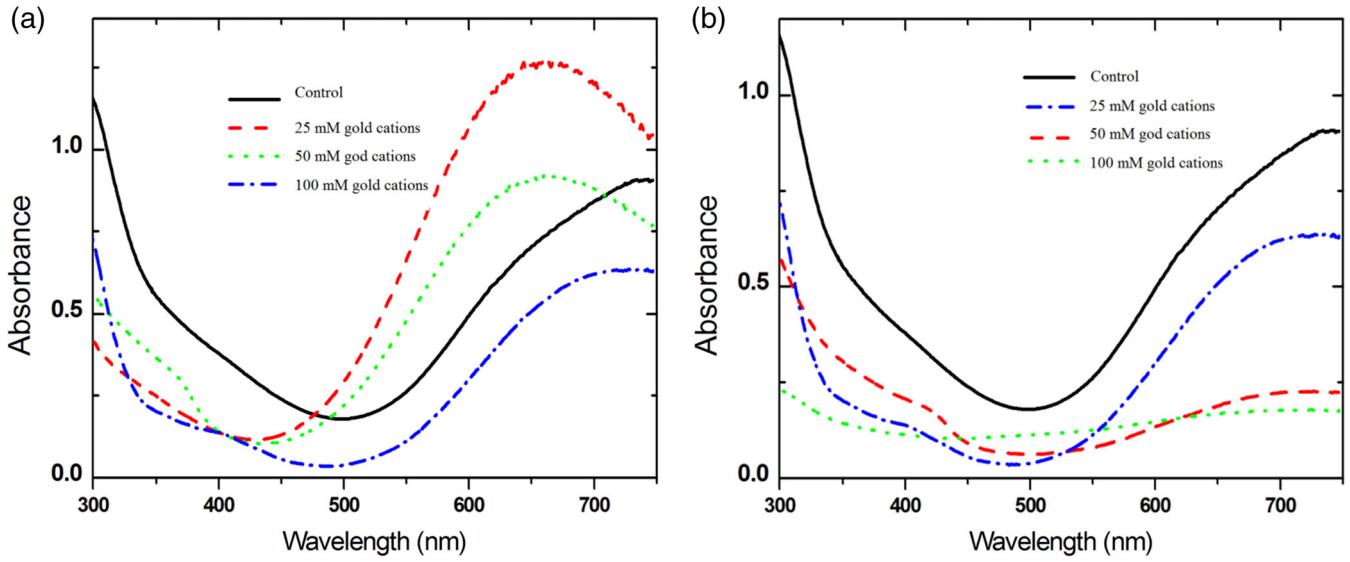

FIGURE 3 (a) UV–VIS spectra of the PBNP-AuNP nanohybrid made through Method 1 (i, ii, and iii) along with the control (PBNPs). (b) UV–VIS spectra of the PBNP-AuNP nanohybrid made through Method 2 (i, ii, and iii) along with the control (PBNPs)

3.3 | Characterization of cationic polymer coated PBNPs and AuNPs

The particle size and morphology of the as-synthesized PBNPs were characterized using TEM analysis (Figure 4a, i). Figure 4a, ii shows the selected area electron diffraction pattern (SAED) of the as-synthesized PBNPs, indicating the excellent crystalline structure of the PBNPs. Figure 4b, i, ii, and iii) shows the TEM images of PBNP-AuNPs made through Method 1; the AuNPs were made with a 50 mM initial concentration of gold cations. The TEM images and the SAED data confirmed the presence of both PBNPs and AuNPs. A similar conclusion is drawn from EDX analysis (shown in Figure 4b, iv, and v). TEM images and SAED data from PBNP-AuNP nanohybrids made through Method 2 from the use of 50 mM gold cations are shown in Figure 4c, i, ii, and iii. The result reveals lower polycrystalline features in PBNP-AuNP nanohybrids made with Method 2 than those made with Method 1. In order to have further insight on the interaction between PBNPs and gold cations, we attempted to make PBNP-AuNPs using a higher amount of

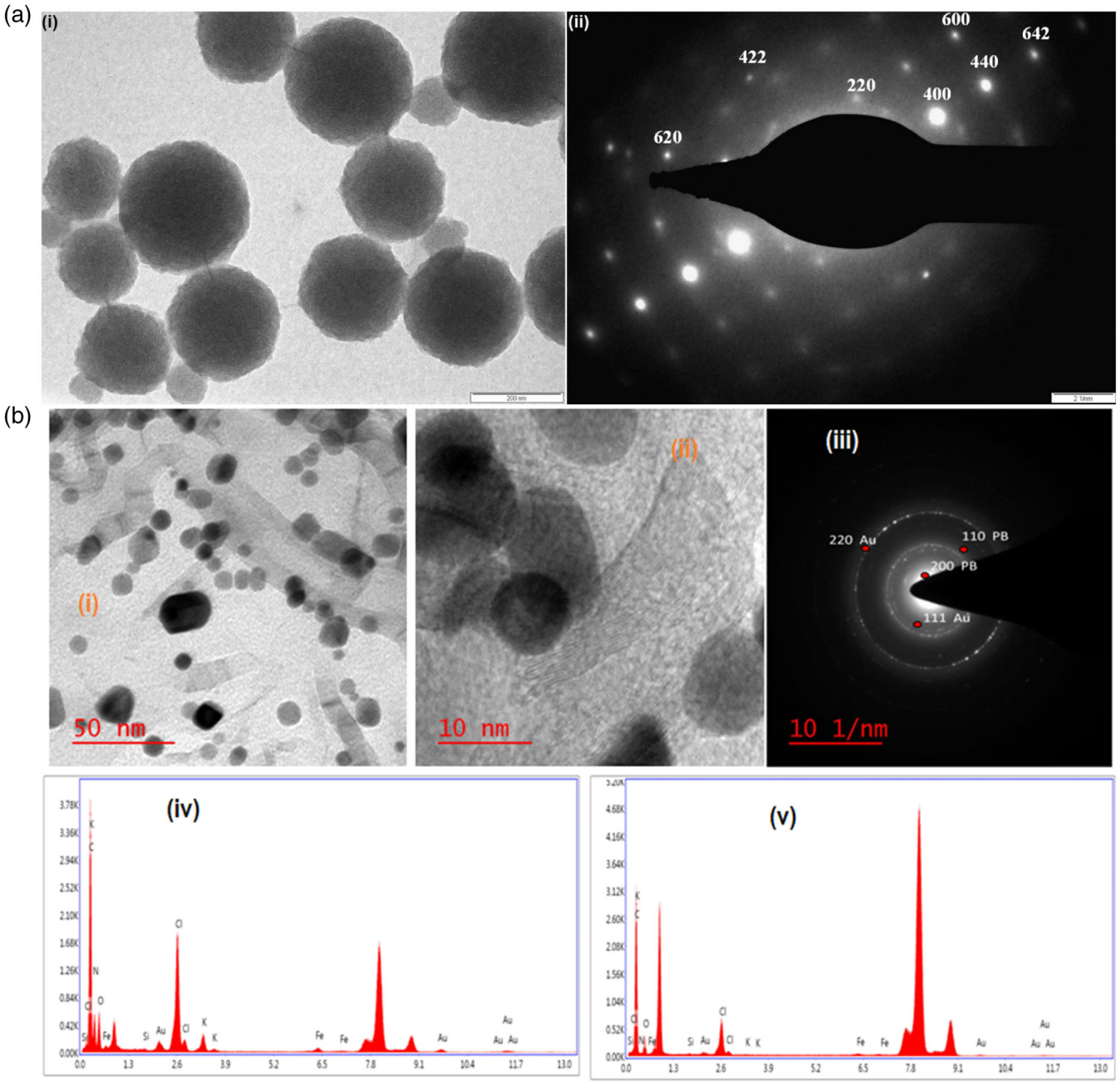

FIGURE 4 (a) (i) TEM image of PBNPs. (ii) Selected area electron diffraction pattern of PEI-protected PB. (iii) TEM image of a selected portion of the image shown in (i). (iv) TEM image of PBNP-AuNP made by mixing PEI-protected PBNPs and AuNPs with PEI as the common reagent and mixed. (b) TEM images of PBNP-AuNPs made through Method 1 with an initial concentration of 50 mM gold cations at two different magnifications (i) and (ii) followed by SAED (iii). (C) TEM images of PBNP-AuNPs made through Method 2 with an initial concentration of 50 mM gold cations (i) followed by SAED (ii). (iii) TEM images with a higher concentration of PB, with a similar concentration of gold cations as recorded in (i, ii); (iv) the respective SAED. (d) XRD patterns of (a) PBNPs and (b) AuNPs assembled PBNPs

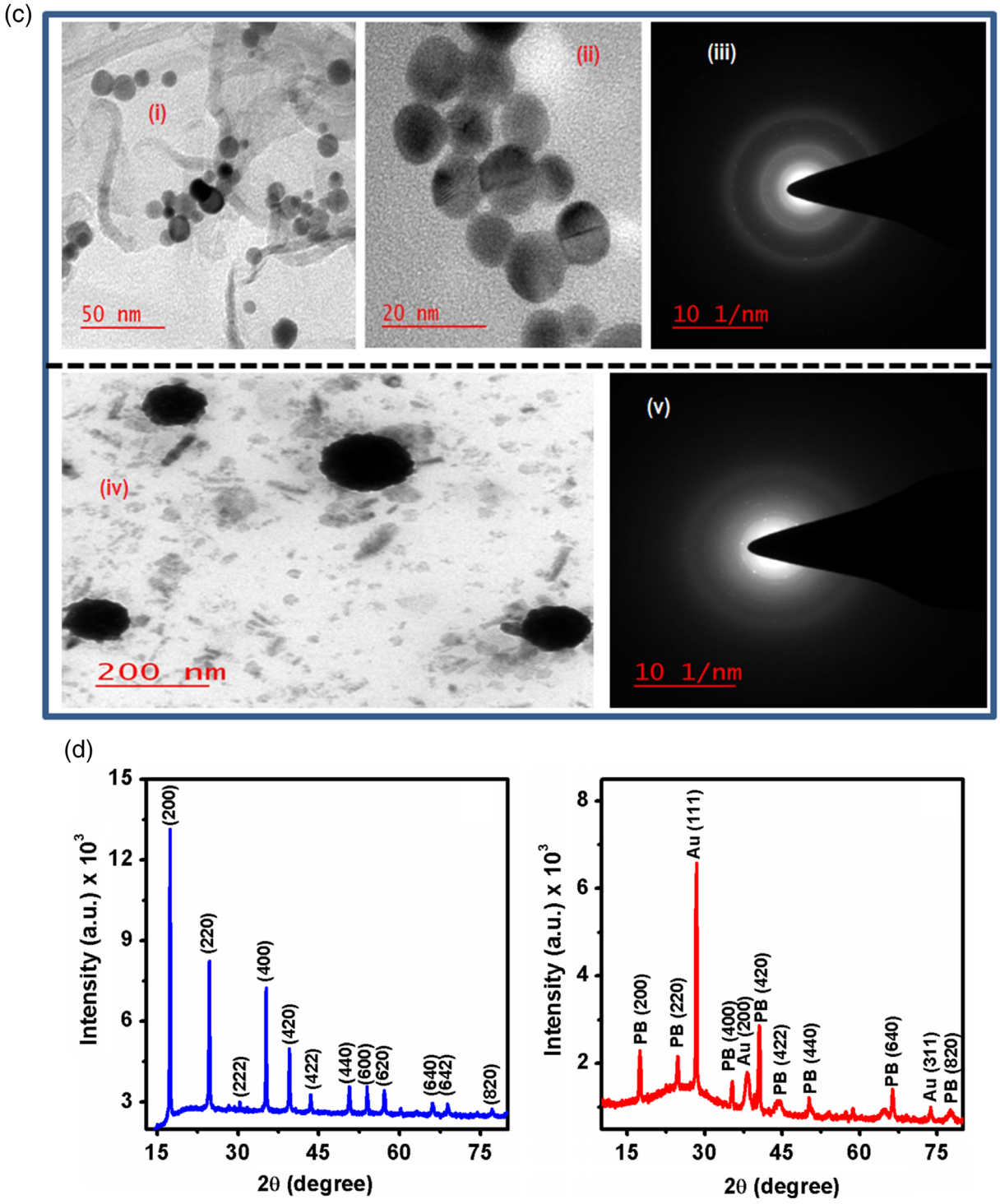

FIGURE 4 (Continued)

PBNPs through Method 2 as compared with what is shown in Figure 4c i, ii, and iii. The results indicate the formation of nanoaggregrate PBNP-AuNPs, followed by further decrease in the polycrystalline structure; these results indicate the structural variation in PBNP morphology.

PBNPs and AuNPs assembled PBNPs were dried at 60°C; the resulting powder was used for XRD analysis. The XRD diffractogram of PBNPs and PBNPs-AuNPs is shown in Figure 4d. X-ray diffraction analysis of the as-synthesized PBNPs shows peaks at ca. 17.4° (200), 24.7° (220), 35.3° (400), 39.6° (420), and 43.7° (422), 50.0° (440), 53.9° (600), 57.2° (620), 66.1° (640), 68.9° (642), and 77.2° (820), which can be indexed as the PB cubic space group Fm3m (Ding et al., 2009; Samain et al., 2013). Figure 3b shows the X-ray diffractogram of AuNPs assembled PBNPs. There are peaks at ca. 28.2°, 38.3°, and 74.2° (2θ value), which can be assigned as (111), (200), and (311), respectively; these peaks correspond to the face-centered cubic (fcc) phase of gold. Along with these peaks, there are a few other peaks in

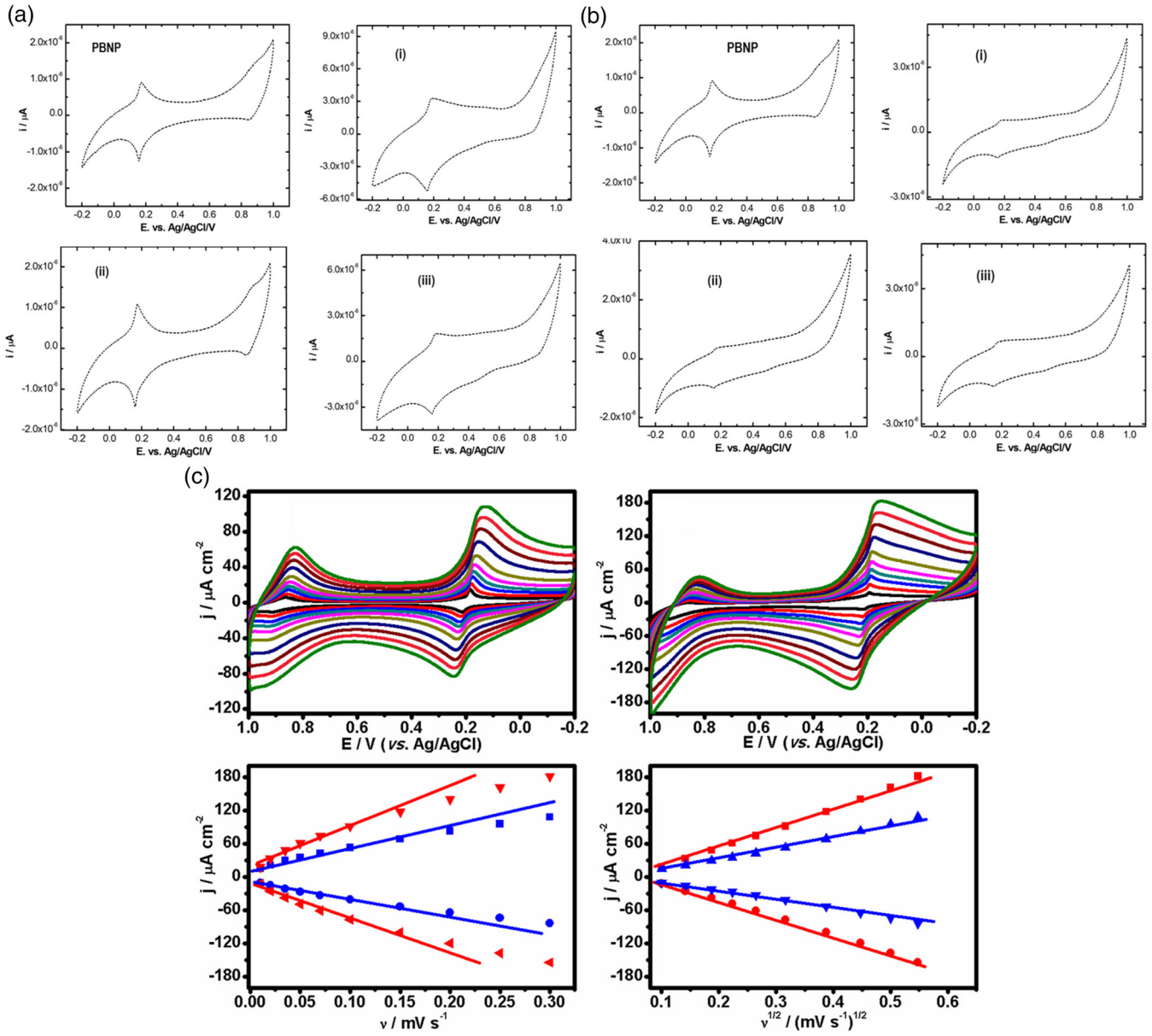

FIGURE 5 (a) Cyclic voltammograms of PBNPs and PBNP-AuNPs in 0.1 M phosphate buffer pH 7.0 containing 0.5 M KCl at a scan rate of 10 mV/s made through Method 1 (i, ii, and iii) along with control (PBNPs); (b) cyclic voltammograms of PBNPs and PBNP-AuNPs made through Method 2 (i, ii, and iii) along with control (PBNPs); (c) Cyclic voltammograms of PBNPs-modified electrode (a) and AuNPs assembled PBNPs-modified electrode (b) in 0.1 M KNO_3 at scan rates of 10, 20, 35, 50, 70, 100, 150, 200, 250, and 300 mV/s, consecutively; (c) the plot of anodic and cathodic current density versus scan rate; and (d) the plot of square root of scan rate versus scan rate

AuNPs assembled PBNPs at ca. 17.6°, 24.8°, 35.5°, 44.3°, 50.4°, 66.1° and 66.1° (2θ value), which can be indexed as the (200), (220), (400), (422), (440), (640), and (820) corresponding to the PB phases.

The synthesis of water-soluble PBNPs involves the use of a hydrophilic polymer with a repeating unit composed of an amine group and a two carbon aliphatic CH_2CH_2 spacer. PEI is a cationic polymer; during nucleation of Prussian blue, the negatively charged centers of PB facilitate stronger attachments through electrostatic attraction, leading to cationic polymer-coated PBNPs.

3.4 | Electrochemistry and catalytic activity of PBNPs and PBNP-AuNP nanohybrid modified electrodes

The PBNP-AuNPs made from Method 1 and Method 2 were characterized via electrochemical measurements. The nanohybrids were adsorbed on graphite powders to make graphite paste electrodes. Figure 5a, i, ii, iii and b, i, ii, iii, shows the cyclic voltammograms of PBNP-AuNP modified electrodes made through Method 1 and

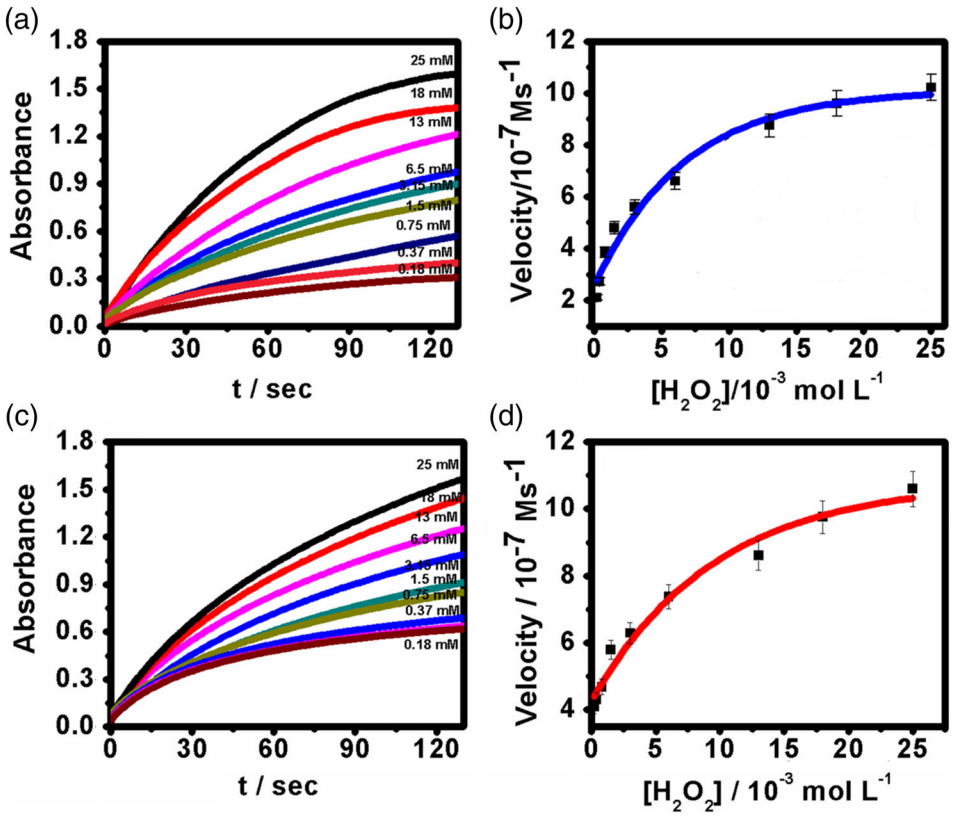

FIGURE 6 Time dependent absorbance changes at 430 nm in the presence of various concentrations of H_2O_2 (from 0.18 to 25 mM) and a fixed concentration of o-dianisidine (50 μM) catalyzed by PBNPs (a) and AuNPs-assembled PBNPs (c). Kinetic analysis of PBNPs (b) and AuNPs assembled PBNPs (d) with H_2O_2 as the substrate

Method 2, respectively, in 0.1 M phosphate buffer containing 0.5 M KCl at the scan rate of 10 mV/s. The two reversible redox couples are affected by the methods used in nanohybrid formation; they were observed between potential ranges of −0.2 to 1.0 V versus Ag/AgCl. The first redox peaks correspond to the oxidation of Prussian white and reduction of PB; the second redox couple at 0.9 V corresponds to the oxidation of PB and reduction of Berlin green (Pandey & Pandey, 2014). The nanohybrid made through Method 1 as shown in Figure 5a, i, ii, iii, iv clearly demonstrates an improvement in PB character as evidenced from redox peaks confirming PB character. However, the nanohybrid made through made through Method 2 show a gradual decrease in the PB character. The findings reveal that the formation of gold hexacyanoferrate predominates rather than the existence of both PBNPs and AuNPs in the nanohybrid made through Method 2. Water-soluble PBNPs display excellent redox electrochemistry as shown in Figure 5c. The self-assembly of AuNPs facilitates both faster oxidation and reduction processes, with a significant increase in the cathodic and anodic current under similar conditions as shown in Figure 5d.

3.5 | Homogeneous catalysis of PBNPs and AuNPs assembled PBNPs

PBNPs and its mixed metal hexacyanoferrate display an analogous behavior to peroxidase; these materials have been studied as a potential replacement for the peroxidase enzyme, which is susceptible to inactivation under various environmental conditions. Accordingly, the development of a peroxidase mimetic that has catalytic activity similar to the peroxidase enzyme is of technical interest. The PBNPs show both homogeneous and heterogeneous catalysis. Figure 6 shows the homogeneous peroxidase-like catalytic activity of PBNPs and PBNPs-AuNPs systems for the o-dianisidine-H_2O_2 chromogenic reaction. The time-dependent absorbance changes at 430 nm in the presence of different concentrations (0.18 to 25 mM) of H_2O_2 and a fixed concentration of o-dianisidine (50 μM) is shown in Figure 6; the enzyme kinetic parameter as Michaelis–Menten constant (km) was calculated. Figure 6a,c show the steady-state kinetic parameters of as-synthesized PBNPs and PBNPs-AuNPs, respectively. Figure 6b,d show that the PBNPs and PBNPs-AuNPs follow Michaelis–Menten kinetics, respectively. The value of K_m was calculated as 2.4 mM for PBNPs and 1.3 mM for PBNPs-AuNPs. The Km for horseradish peroxidase has been reported to 3.68 mM. The kinetic parameter was calculated as 1.3 mM for PBNP-AuNPs, indicating the advantage of the as-made material as a substitute for peroxidase; a high value of K_m indicates a weaker affinity of the substrate to the enzyme and a low value of K_m implies a higher affinity of the substrate to the enzyme.

3.6 | PBNPs/PBNP-AuNP mediated reduction of H_2O_2

An earlier study demonstrated that H_2O_2 undergoes both direct electrocatalytic and HRP-mediated reduction at lower potential (Pandey, Upadhyay, Tiwari, & Tripathi, 2001). In order to resolve the variation in the catalytic ability of PBNPs and AuNPs assembled PBNPs, cyclic voltammograms of graphite paste electrodes modified with these

materials were examined in the absence and the presence of 1 mM H_2O_2. The results recorded for the PBNPs are shown in Figure 7a and for the AuNPs assembled PBNPs are shown in Figure 7b. Catalytic reduction of H_2O_2 was examined at 0.2 V versus Ag/AgCl for PBNPs and self-assembled AuNPs on PBNPs (Figure 7b). The electrocatalytic performance of PBNPs and AuNPs assembled PBNPs was also evaluated using amperometric measurements under stirring conditions in a 0.1 M phosphate buffer solution containing 0.5 M KCl (pH = 7.0). The catalytic activity was significantly improved after AuNPs assembly as shown the from amperograms (Figure 7c). The sensitivity of the PBNPs and AuNPs assembled PBNPs modified-electrodes for H_2O_2 analysis was found to be 34.7 and 84.9 μA mM^{-1} cm^{-2}; the lowest detection limit were 200 and 50 nM, respectively. These findings confirmed the role of AuNPs assembled PBNPs on the electrocatalytic reduction of H_2O_2 and revealed that nanostructured AuNPs significantly enhance the dynamics of H_2O_2 reduction. Findings similar to those for homogeneous catalysis were obtained, justifying the usability of the as-made materials for both homogeneous and heterogeneous systems. The catalytic rate constant (K_{cat}) for PBNPs and PBNPs-AuNPs mediated reduction of H_2O_2 was investigated as described earlier (Windmiller, Valdés-Ramírez, et al., 2011) using following relationship:

$$I_{cat}/I_L = (K_{cat}\, Ct)^{1/2}$$

In this equation, I_{cat} and I_L are the currents of the PBNPs modified electrodes in the presence and absence of H_2O_2, respectively. K_{cat} was calculated from the slope of the Icat/I_L versus $t^{1/2}$ plot. Figure 8a,b show the chronoamperograms of the PBNPs and PBNPs-AuNPs systems, respectively, in the presence and absence of 1 mM H_2O_2. The values for K_{cat} were calculated to be 2.42×10^2 M/s and 5.78×10^2 M/s for PBNPs and PBNPs-AuNPs, respectively. These results suggest potential applications of the as-made materials in electroanalytical chemiatry.

3.7 | PBNPs/PBNPs-AuNPs mediated oxidation of H_2O_2

The electrocatalytic oxidation of H_2O_2 has also been studied at the surface of the modified electrode. H_2O_2 undergoes oxidation at a relatively high potential (Li, Yu, & Peng, 2005). The PB system described to this point catalyzes the oxidation of H_2O_2 at a high potential (0.9 V vs. Ag/AgCl) with relatively low sensitivity (Jaffari & Pickup, 1996; Karyakin, Gitelmacher, & Karyakina, 1995). We assessed the

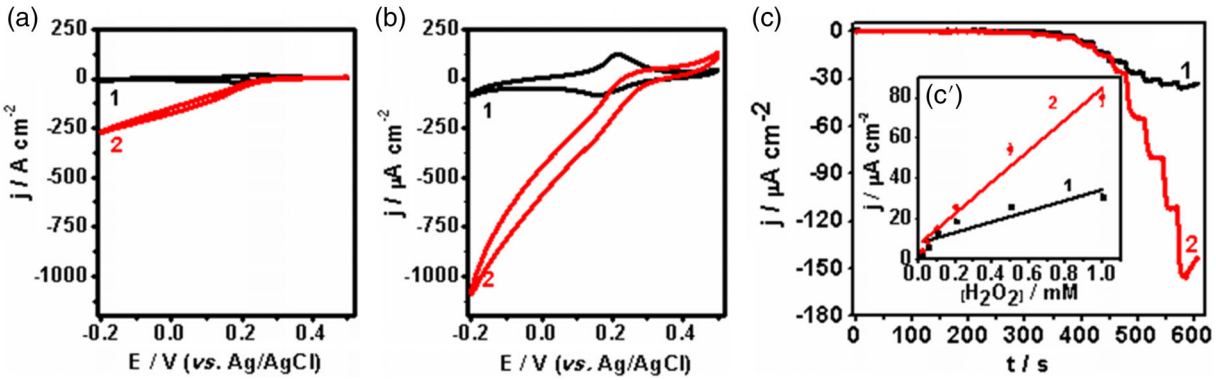

FIGURE 7 Cyclic voltammograms of PBNPs (a) and AuNPs assembled PBNPs (b) in the absence (1) and the presence (2) of 1 mM H_2O_2 at a scan rate of 0.01 V s^{-1} in 0.1 M phosphate buffer (pH 7.0) containing 0.5 M KCl. (c) Amperometric response of PBNPs (1) and AuNPs-PBNPs (2) modified electrodes at 0.2 V versus Ag/AgCl after the addition of various concentrations of H_2O_2

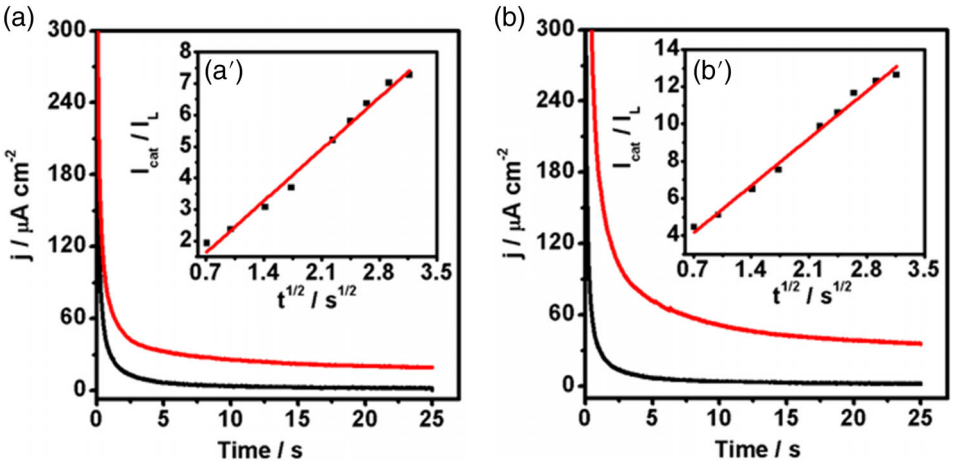

FIGURE 8 Chronoamperograms for (A) PBNPs and (B) PBNPs-AuNPs modified electrode in the absence (black curve) and in the presence (red curve) of 1 mM H_2O_2. A step potential of −0.05 V versus Ag/AgCl was used in this study. The inset shows the corresponding plots of I_{cat}/I_L versus $t^{1/2}$ in 0.1 M phosphate buffer containing 0.5 M KCl as the supporting electrolyte

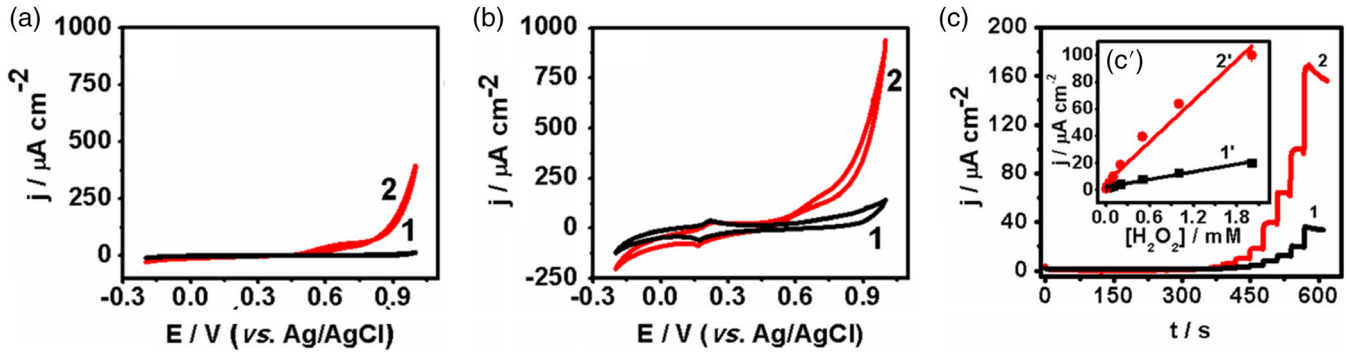

FIGURE 9 Cyclic voltammograms of PBNPs (a) and AuNPs assembled PBNPs (b) in the absence (i) and the presence (ii) of 1 mM H_2O_2 at the scan rate of 0.01 V s^{-1} in 0.1 M phosphate buffer solution (pH 7.0) containing 0.5 M KCl. (c) Amperometric response of corresponding PBNPs (1) and AuNPs-PBNPs (2) at 0.6 V versus Ag/AgCl on the addition of various concentrations of H_2O_2

TABLE 1 Electrocatalytic performance of various modified electrodes toward H_2O_2 detection

Working electrode	Applied potential/ V (vs. ag/AgCl)	Linear range (μM)	Sensitivity (μA mM^{-1} cm^{-2})	Detection limit (μM)	Reference
ITO/TiO_2 film/PB	0.0	Nr	257	0.01	(Li et al., 2005)
GE/PBNPs/Nafion	−0.05	2.1–140	138.6	1	(Karyakin et al., 1995)
Pt/SAPB	−0.05	1–400	625	Nr	(Jaffari & Pickup, 1996)
CPE/FMCA-sol–gel-HRP	−0.10	Nr	30	Nr	(Wang et al., 2017)
GCE/graphene/PB	−0.05	20–200	196.6	1.9	(Aller-Pellitero et al., 2019)
PB-$AuNP_2$-Pd_2	0.0	50–1,000	323.1	0.1	(Qiu et al., 2007)
PB-$AuNP_2$-Pd_2	+0.2	50–1,000	17.25	0.1	(Qiu et al., 2007)
CPE/PB	+0.2	Nr	41.26	Nr	(Qiu et al., 2007)
CPE/PB-$AuNP_1$	+0.2	Nr	4.13	Nr	(Qiu et al., 2007)
PB-AuNP2	+ 0.2	Nr	8.65	Nr	(Qiu et al., 2007)
CPE/PBNPs	+0.2	50–1,000	34.7	0.2	This work
CPE/AuNPs-PBNPs	+0.2	50–1,000	84.9	0.05	This work
CPE/PBNPs	+0.6	50–2000	12.0	20	This work
CPE/AuNPs-PBNPs	+0.6	2–2000	56	5	This work

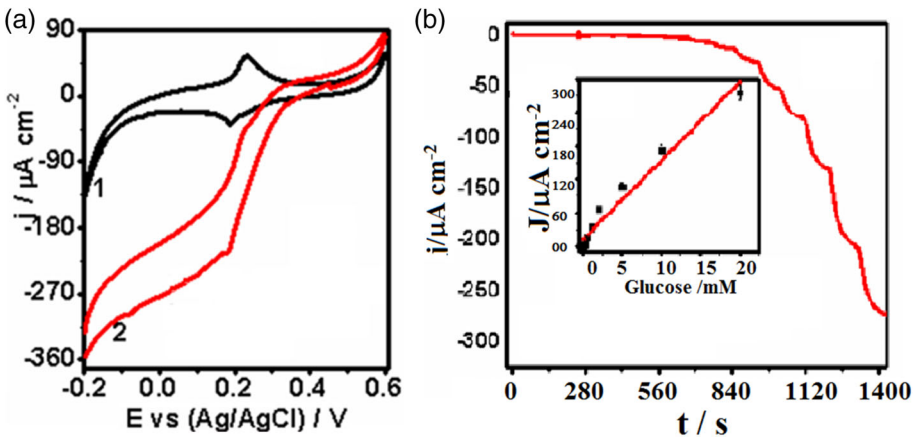

FIGURE 10 (a) Cyclic voltammogram of the PBNP-AuNP nanocomposite and the glucose oxidase-modified electrode in the absence (1) and the presence of 500 mM glucose. (b) Amperometric response of the enzyme-modified electrode on the addition of various concentrations of glucose at 0.2 V versus Ag/AgCl

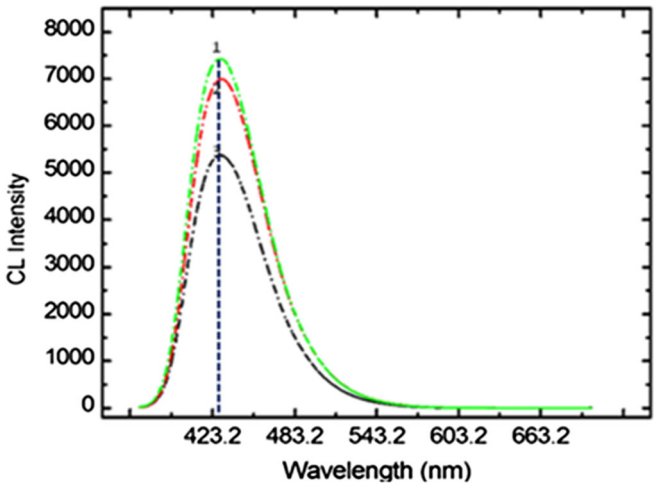

FIGURE 11 Luminescent ability of luminol-H_2O_2-glucose oxidase and glucose biointerface in the presence of (1) PBNP-AuNP made through Method 1, (2) PBNP-AuNP made through Method 2, and (3) only PBNPs

electrocatalytic oxidation of H_2O_2 at a relatively low potential (i.e., 0.6 V vs. Ag/AgCl) on the PBNPs or AuNPs assembled PBNPs modified graphite paste electrodes (Figure 9).

We found that the as-made material efficiently catalyzed the oxidation of H_2O_2 at 0.6 V versus Ag/AgCl for sensitive detection of H_2O_2 (Figure 9a). The sensitivity of the PBNPs and PBNPs-AuNPs modified electrodes for H_2O_2 analysis were shown to be 12 and 56 μA mM^{-1} cm^{-2}, respectively. The lowest detection limits of the PBNPs and PBNPs-AuNPs modified electrodes were shown to be were shown to be 20 and 5 μM, respectively. The co-operative self-assembly of AuNPs further enhances the catalytic activity, increasing the sensitivity of the sensing-based anodic current measurement (Figure 9b). A comparison of the electrocatalytic behaviour of the as-made material with those reported earlier is shown in Table 1. The results reveal the advantages of the as-made materials over those reported previously.

3.8 | Probing of glucose oxidase-catalyzed reaction

The electrochemical behavior of a glucose oxidase enzyme-modified electrode made from the PBNP-AuNP nanocomposite was examined by cyclic voltammetry as shown in Figure 10a. Measurements were obtained in the absence and presence of 500 mM glucose; a scan rate of 5 mV/s was used in this study. There were significant increases in cathodic current when glucose was added; this result shows the efficient sensing of glucose through the glucose oxidase- catalyzed reaction. The findings were further examined through amperometric measurements at 0.1 V versus Ag/AgCl on the addition of various concentrations of glucose (as shown in Figure 10b). Excellent amperometric detection of glucose was recorded, confirming the efficient catalytic ability of this material.

3.9 | Chemical characterization of the luminol-H_2O_2 biointerface

The luminol-H_2O_2 system has been explored in many bioassays; this approach involves luminescence measurements of the formation of hydrogen peroxide as a function of an oxidase-catalyzed reaction (Wang et al., 2017). In this study, the luminol-H_2O_2 biointerface was used to detect catalytic activity of glucose oxidase in the presence of glucose. The luminol-H_2O_2 biointerface was used to evaluate the catalytic activity of PBNPs and PBNP-AuNP nanohybrids, which act as peroxidase mimetic materials. The catalytic influence of PBNP/PBNP-AuNPs made by Method 1 and Method 2 was assessed by evaluating the luminescence intensity of luminol-H_2O_2 biointerface; the results obtained using this approach are shown in Figure 11. The results reveal that the PBNP-AuNP nanohybrids made by Method 1 shows enhanced chemiluminescence as compared with those made by Method 2 and PBNPs.

3.10 | Reproducibility and selectivity of PBNPs and PBNP-AuNP nanohybrid modified electrodes on electrochemical biosensing

The PBNPs are an excellent peroxidase mimetic, which allows for selective reduction of hydrogen peroxide. We investigated on the reproducibility of PBNP/PBNP-AuNP-modified electrodes by evaluating 10 electrodes of analogous design that were made under similar conditions. The reproducibility in terms of sensitivity on the order of 97% was recorded for each set of the modified electrodes. This result confirmed the utility of nanomaterial for sensing applications.

3.11 | Portable microneedle-based electrochemical sensors

An earlier study demonstrated the fabrication of electrochromic biosensors based on a screen printed electrode for both colorimetric and amperometric sensing (Aller-Pellitero et al., 2019) The PB modified screen printed electrode was prepared using a screen printable paste, which was made from a chemically synthesized PB nanocomposite. Indium tin oxide or Sb-doped SnO_2 (ATO) particles and chemically synthesized Prussian blue obtained from the co-precipitation of two precursors were mixed with binder to make the screen printable PB paste. The behavior of the PB in this nanocomposite may not be appropriate for colorimetric or electrochemical sensing. In addition, as made PB [36] is difficult to process and cannot meet the requirements of colorimetric and electrochemical sensing independently. Accordingly, we made processable PEI-protected Prussian blue nanoparticles that can be either used for colorimetric sensing or may be dispensed over the working portion of a screen printed electrode to develop a PB-based screen printed electrode for biosensing. The performance of as made PB/PB-AuNP modified screen printed electrode is shown in Table 2.

TABLE 2 Comparison of different Prussian-blue based amperometric sensors/biosensors

Electrode	Preparation of PB/nanocomposite	Analyte	LOD	Range	Sensitivity	References
SPEs	Undisclosed	Uric acid	3 μM	10–200 μM	0.89 A cm^{-2} M^{-1}	(da Cruz, de Souza Paula, Franco, dos Santos, & Ferreira, 2017)
SPEs	Undisclosed	Catechol	0.1 μM	1–90 μM	Unreported	(Buleandra et al., 2014)
SPEs	Undisclosed	Paraoxon	12 μM	5–150 μM	Unreported	(Scognamiglio et al., 2012)
SPEs	Undisclosed	Ethanol	12 μM	20 μM	0.05–0.5 mM	(Rama et al., 2012)
SPEs	Undisclosed	Glucose	Unreported	0–33.1 mM	5.8×10^{-4} A cm^{-2} M^{-1}	(Noiphung et al., 2013)
SPEs	Undisclosed	H_2O_2	3.6 μM	0–100 μM	0.1 A cm^{-2} M^{-1}	(Dungchai, Chailapakul, & Henry, 2009)
		Glucose	0.7 mM	0–100 mM	4.8×10^{-3} A cm^{-2} M^{-1}	
		Uric acid	4.6 mM	0–35 mM	4.5×10^{-4} A cm^{-2} M^{-1}	
		Lactate	1.19 mM	0–50 mM	3.0×10^{-3} A cm^{-2} M	
SPEs	Undisclosed	Lactate	0.15 μM	0.15 μM–1.1 mM	0.4 A cm^{-2} M^{-1}	(Shimomura et al., 2012)
Carbon SPEs	PB drop casted on C SPEs	Cysteine	98.9 μM	300–700 μM	0.06 A cm^{-2} M^{-1}	(Bonacin et al., 2018)
PB/carbon SPEs	PB incorporated in C paste	Cysteine	64.4 μM	100–600 μM	0.09 A cm^{-2} M^{-1}	(Cinti et al., 2018)
SiO_2-ATO/PB	Growth of particle on SiO_2-ATO	H_2O_2	3.8 mM	0.025–5 mM	0.07 A cm^{-2} M^{-1}	(Aller-Pellitero et al., 2019)
ITO/PB	Growth of particle on ITO	H_2O_2	3.2 mM	0.015–5 mM	0.08 A cm^{-2} M^{-1}	(Aller-Pellitero et al., 2019)
SiO_2-ATO/PB	Growth of particle on SiO_2-ATO	Glucose	54.1 μM	0.1–1 mM	8.8×10^{-3} A cm^{-2} M	(Aller-Pellitero et al., 2019)
ITO/PB	Growth of particle on ITO	Glucose	7.5 μM	0.1-1 mM	7.4×10^{-3} A cm^{-2} M	(Aller-Pellitero et al., 2019)
PB dispensed on SPE	PEI protected processable PB	H_2O_2	10 μM	0.1–10 mM	12 μA mM^{-1} cm^{-2}	This work
PB-AuNP dispensed on SPE	PEI protected processable PB-AuNP	H_2O_2	1 μM	0.1–10 mM	56 μA mM^{-1} cm^{-2}	This work
PB dispensed on SPEs	PEI protected processable PB	Glucose	15 μM	0.1–10 mM	15×10^{-3} A cm^{-2} M	This work
PB-AuNP dispensed on SPEs	PEI protected processable PB-AuNP	Glucose	3 μM	0.05–10 mM	30×10^{-3} A cm^{-2} M	This work

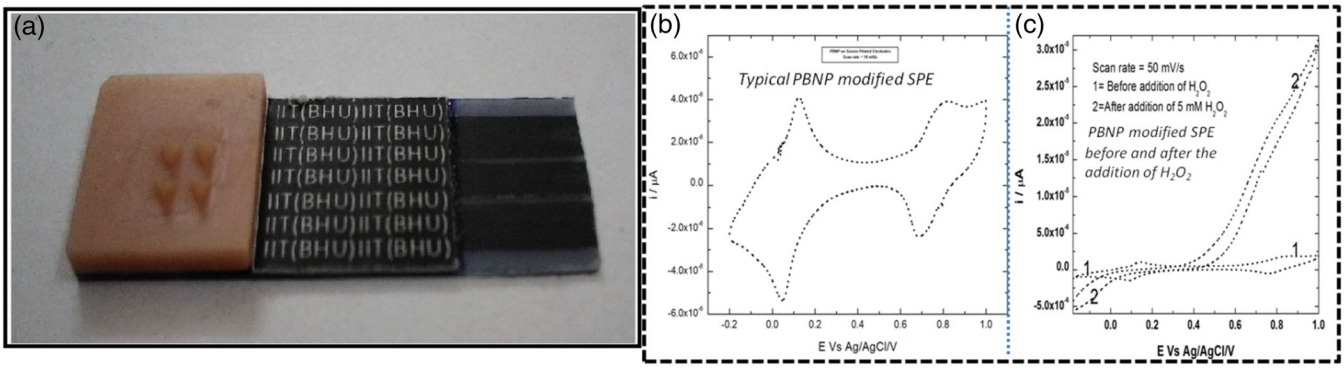

FIGURE 12 (a) Microneedle-assembled screen-printed electrode, cyclic voltammograms of screen-printed electrode (b) before and (c) after the addition of 1 mM hydrogen peroxide

FIGURE 13 Portable microneedle-based electrochemical sensor for detection of hydrogen peroxide levels

Here, we explored integration of hollow microneedles with screen-printed electrodes (SPE) containing graphite working electrode and counter electrodes and Ag/AgCl reference electrode. The Prussian blue-gold nanoparticles nanohybrid was dispensed over the working electrode of the freshly prepared screen-printed electrode; the hollow microneedle array was assembled over this construct (Figure 12a). The electrochemical performance of microneedle assembled SPE is shown Figure 12b; this result represents the redox activity of as made Prussian blue nanoparticles described above. The microneedle-based sensor responded well to hydrogen peroxide (as shown in Figure 12c). This result confirmed the change in both cathodic and anodic current after the addition of hydrogen peroxide (Figure 7). As shown in Figure 13, the system has been further updated by the incorporation of a dedicated electrochemical detector that can be programmed for detecting an enzymatic reaction resulting in the formation of hydrogen peroxide. We are further innovating the printing technology to incorporate temporary tattoos that attach to the skin.

4 | CONCLUSIONS

In summary, we showed that PEI enables the formation of water-soluble cationic polymer-coated PBNPs from a single precursor. The cationic coating allows for cooperative self-assembly of in situ generated AuNPs. These materials provide better catalytic activity than the peroxidase enzyme-catalyzed reaction based for both reduction and oxidation of hydrogen peroxide. PEI-mediated synthesis of water soluble PBNPs was also demonstrated. The magnetic property studies showed that the as-synthesized PBNPs displayed superparamagnetism. This approach can be utilized for the formation PBNP-AuNP nanohybrids, in which the PB character can be precisely manipulated by embedding AuNPs along with PBNPs within the nanohybrids. A gradually decrease in PBNP behavior was associated with the formation of PBNP-Au nanoaggregrates. PBNP-Au nanocomposite behaves as an efficient electrocatalyst for glucose oxidase-catalyzed detection of glucose. Chemical characterization of the luminol-H_2O_2 biointerface was evaluated in the presence of PBNP and PBNP-AuNP nanohybrids. The presence of AuNPs in the nanohybrid significantly enhances the chemiluminescence of the luminol-H_2O_2 biointerface. PBNPs may be used for probing glucose oxidase-catalyzed reactions and many other oxidase enzyme reactions. These innovative materials have many potential biomedical applications, including use in the detection of glucose and other biologically-relevant molecules.

ACKNOWLEDGMENTS

The authors would like to acknowledge support from the Department of Science and Technology's VAJRA (Visiting Advanced Joint Research) Faculty award through Grant Number VJR-2017-000034 to Roger J. Narayan, which facilitated interaction between the Indian and US institutions.

REFERENCES

Aller-Pellitero, M., Fremeau, J., Villa, R., Guirado, G., Lakard, B., Hihn, J. Y., & Del Campo, F. J. (2019). Electrochromic biosensors based on screen-printed Prussian blue electrodes. *Sensors and Actuators B: Chemical*, *290*, 591–597.

Buleandra, M., Rabinca, A. A., Mihailciuc, C., Balan, A., Nichita, C., Stamatin, I., & Ciucu, A. A. (2014). Screen-printed Prussian blue modified electrode for simultaneous detection of hydroquinone and catechol. *Sensors and Actuators B*, *203*, 824–832.

Bonacin, J. A., Dos Santos, P. L., Katic, V., Foster, C. W., & Banks, C. E. (2018). Use of screen-printed electrodes modified by prussian blue and analogues in sensing of cysteine. *Electroanalysis*, *30*(1), 170–179.

Cinti, S., Cusenza, R., Moscone, D., & Arduini, F. (2018). based synthesis of Prussian Blue Nanoparticles for the development of whole blood glucose electrochemical biosensor. *Talanta*, *187*, 59–64.

da Cruz, F. S., de Souza Paula, F., Franco, D. L., dos Santos, W. T. P., & Ferreira, L. F. (2017). Electrochemical detection of uric acid using graphite screen-printed electrodes modified with Prussian blue/poly (4-aminosalicylic acid)/Uricase. *Journal of Electroanalytical Chemistry*, *806*, 172–179.

Ding, Y., Hu, Y.-L., Gu, G., & Xia, X.-H. (2009). Controllable synthesis and formation mechanism investigation of Prussian blue nanocrystals by using the polysaccharide hydrolysis method. *Journal of Physical Chemistry C*, *113*, 14838–14843.

Dungchai, W., Chailapakul, O., & Henry, C. S. (2009). Electrochemical detection for paper-based microfluidics. *Analytical Chemistry*, *81*, 5821–5826.

Entley, W. R., & Girolami, G. S. (1995). High-temperature molecular magnets based on Cyanovanadate building blocks: Spontaneous magnetization at 230 K. *Science*, *268*, 397–400.

Ferlay, S., Mallah, T., Ouahes, R., Veillet, P., & Verdaguer, M. (1995). A room-temperature organometallic magnet based on Prussian blue. *Nature*, *378*, 701–703.

Gittard, S. D., Miller, P. R., Boehm, R. D., Ovsianikov, A., Chichkov, B. N., Heiser, J., … Narayan, R. J. (2010). Multiphoton microscopy of transdermal quantum dot delivery using two photon polymerization-fabricated polymer microneedles. *Faraday Discussions*, *149*, 171.

Gittard, S. D., Ovsianikov, A., Chichkov, B. N., Doraiswamy, A., & Narayan, R. J. (2010). Two photon polymerization of microneedles for transdermal drug delivery. *Expert Opinion on Drug Delivery*, *7*, 1.

Gittard, S. D., Ovsianikov, A., Monteiro-Riviere, N. A., Lusk, J., Morel, P., Minghetti, P., … Narayan, R. J. (2009). Fabrication of polymer microneedles using a two-photon polymerization and Micromolding process. *Journal of Diabetes Science and Technology*, *3*, 304–311.

Holmes, S. M., & Girolami, G. S. (1999). Sol−gel synthesis of KVII[CrIII(CN)6]·2H2O: A crystalline molecule-based magnet with a magnetic ordering temperature above 100 °C. *Journal of the American Chemical Society*, *121*, 5593–5594.

Jaffari, S. A., & Pickup, J. C. (1996). Novel hexacyanoferrate (III)-modified carbon electrodes: Application in miniaturized biosensors with potential for in vivo glucose sensing. *Biosensors & Bioelectronics*, *11*, 1167–1175.

Jing, L., Liang, X., Deng, Z., Feng, S., Li, X., Huang, M., … Dai, Z. (2014). Prussian blue coated gold nanoparticles for simultaneous photoacoustic/CT bimodal imaging and photothermal ablation of cancer. *Biomaterials*, *35*, 5814–5821.

Karyakin, A. A., Gitelmacher, O. V., & Karyakina, E. E. (1995). Prussian blue-based first-generation biosensor. A sensitive amperometric electrode for glucose. *Analytical Chemistry*, *67*, 2419–2423.

Kaye, S. S., & Long, J. R. (2005). Hydrogen storage in the dehydrated Prussian blue analogues M3[co(CN)6]2(M = Mn, Fe, co, Ni, cu, Zn). *Journal of the American Chemical Society*, *127*, 6506–6507.

Keihan, A. H., Karimi, R. R., & Sajjadi, S. (2020). Wide dynamic range and ultrasensitive detection of hydrogen peroxide based on beneficial role of gold nanoparticles on the electrochemical properties of prussian blue. *Journal of Electroanalytical Chemistry*, *862*, 114001.

Li, J., Yu, Q., & Peng, T. (2005). Electrocatalytic oxidation of hydrogen peroxide and cysteine at a glassy carbon electrode modified with platinum nanoparticle-deposited carbon nanotubes. *Analytical Sciences*, *21*, 377–381.

Miller, P., Moorman, M., Manginell, R., Ashlee, C., Brener, I., Wheeler, D., … Polsky, R. (2016). Towards an integrated microneedle Total analysis Chip for protein detection. *Electroanalysis*, *28*, 1305–1310.

Miller, P. R., Gittard, S. D., Edwards, T. L., Lopez, D. M., Xiao, X., Wheeler, D. R., … Narayan, R. J. (2011). Integrated carbon fiber electrodes within hollow polymer microneedles for transdermal electrochemical sensing. *Biomicrofluidics*, *5*, 013415.

Miller, P. R., Narayan, R. J., & Polsky, R. (2016). Microneedle-based sensors for medical diagnosis. *Journal of Materials Chemistry B*, *4*, 1379–1383.

Miller, P. R., Xiao, X., Brener, I., Burckel, D. B., Narayan, R., & Polsky, R. (2014). Microneedle-based transdermal sensor for on-Chip potentiometric determination of K+. *Advanced Healthcare Materials*, *3*, 876–881.

Noiphung, J., Songjaroen, T., Dungchai, W., Henry, C. S., Chailapakul, O., & Laiwattanapaisal, W. A. (2013). Electrochemical detection of glucose from whole blood using paper-based microfluidic devices. *Analytica Chimica Acta*, *788*, 39–45.

Pandey, P. C., & Panday, D. (2016). Tetrahydrofuran and hydrogen peroxide mediated conversion of potassium hexacyanoferrate into Prussian blue nanoparticles: Application to hydrogen peroxide sensing. *Electrochimica Acta*, *190*, 758–765.

Pandey, P. C., & Pandey, A. K. (2013a). Novel synthesis of Prussian blue nanoparticles and nanocomposite sol: Electro-analytical application in hydrogen peroxide sensing. *Electrochimica Acta*, *87*, 1–8.

Pandey, P. C., & Pandey, A. K. (2013b). Novel synthesis of super peroxidase mimetic polycrystalline mixed metal hexacyanoferrates nanoparticles dispersion. *Analyst*, *138*, 2295–2301.

Pandey, P. C., & Pandey, A. K. (2014). Tetrahydrofuran hydroperoxide mediated synthesis of Prussian blue nanoparticles: A study of their electrocatalytic activity and intrinsic peroxidase-like behavior. *Electrochimica Acta*, *125*, 465–472.

Pandey, P. C., Pandey, G., & Narayan, R. J. (2017a). Controlled synthesis of polyethylenimine coated gold nanoparticles: Application in glutathione sensing and nucleotide delivery. *Journal of Biomedial Materials Research Part B Applied Biomaterials*, *105B*, 1191.

Pandey, P. C., Pandey, G., & Narayan, R. J. (2017b). Polyethylenimine-mediated synthetic insertion of gold nanoparticles into mesoporous silica nanoparticles for drug loading and biocatalysis. *Biointerphases*, *12*, 011005.

Pandey, P. C., Upadhyay, S., Tiwari, I., & Tripathi, V. S. (2001). An ormosil-based peroxide biosensor — A comparative study on direct electron transport from horseradish peroxidase. *Sensors and Actuators B: Chemical*, *72*, 224–232.

Qiu, J.-D., Peng, H.-Z., Liang, R.-P., Li, J., & Xia, X.-H. (2007). Synthesis, characterization, and immobilization of Prussian blue-modified au nanoparticles: Application to electrocatalytic reduction of H_2O_2. *Langmuir*, *23*, 2133–2137.

Rama, E. C., Biscay, J., Garcia, M. B. G., Reviejo, A. J., Carrazon, J. M. P., & Garcia, A. C. (2012). Comparative study of different alcohol sensors based on screen-printed carbon electrodes. *Analytica Chimica Acta*, *728*, 69–76.

Samain, L., Grandjean, F., Long, G. J., Martinetto, P., Bordet, P., Sanyova, J., & Strivay, D. (2013). Synthesis and fading of eighteenth-century Prussian blue pigments: A combined study by spectroscopic and diffractive techniques using laboratory and synchrotron radiation sources. *Journal of Synchrotron Radiation*, *20*, 460–473.

Sato, O., Iyoda, T., Fujishima, A., & Hashimoto, K. (1996). Photoinduced magnetization of a cobalt-iron cyanide. *Science*, *272*, 704–705.

Scognamiglio, V., Pezzotti, I., Pezzotti, G., Cano, J., Manfredonia, I., Buonasera, K., … Giardi, M. T. (2012). Towards an integrated biosensor array for simultaneous and rapid multi-analysis of endocrine disrupting chemicals. *Analytica Chimica Acta*, *751*, 161–170.

Shatruk, M., Dragulescu-Andrasi, A., Chambers, K. E., Stoian, S. A., Bominaar, E. L., Achim, C., & Dunbar, K. R. (2007). Properties of Prussian blue materials manifested in molecular complexes: Observation of cyanide linkage isomerism and spin-crossover behavior in Pentanuclear cyanide clusters. *Journal of the American Chemical Society*, *129*, 6104–6116.

Shimomura, T., Sumiya, T., Ono, M., Itoh, T., & Hanaoka, T. A. (2012). An electrochemical biosensor for the determination of lactic acid in expiration. *Procedia Chemistry*, *6*, 46–51.

Skoog, S. A., Miller, P. R., Boehm, R. D., Sumant, A. V., Polsky, R., & Narayan, R. J. (2015). Nitrogen-incorporated ultrananocrystalline

diamond microneedle arrays for electrochemical biosensing. *Diamond and Related Materials*, *54*, 39–46.

Sun, X., Dong, S., & Wang, E. (2004). One-step synthesis and characterization of polyelectrolyte-protected gold nanoparticles through a thermal process. *Polymer*, *45*, 2181–2184.

Wang, M., & Kan, X. (2018). Multilayer sensing platform: Gold nanoparticles/prussian blue decorated graphite paper for NADH and H_2O_2 detection. *Analyst*, *143*, 5278–5284.

Wang, S., Cazelles, R., Wei-Ching, L., Va ´ zquez-Gonza ´ lez, M., Zoabi, A., Abu-Reziq, ´. R., & Willner, I. (2017). Mimicking horseradish peroxidase and NADH peroxidase by heterogeneous Cu2 +-modified graphene oxide nanoparticles. *Nano Letters*, *17*, 2043–2048.

Windmiller, J. R., Valdés-Ramírez, G., Zhou, N., Zhou, M., Miller, P. R., Jin, C., … Wang, J. (2011). Bicomponent microneedle Array biosensor for minimally-invasive glutamate monitoring. *Electroanalysis*, *23*, 2302–2309.

Windmiller, J. R., Zhou, N., Chuang, M. C., Ramírez, G. V., Santhosh, P., Miller, P. R., … Wang, J. (2011). Microneedle array-based carbon paste amperometric sensors and biosensors. *The Analyst*, *136*, 1846–1851.

Zhai, J., Zhai, Y., Wang, L., & Dong, S. (2008). Rapid synthesis of polyethylenimine-protected Prussian blue Nanocubes through a thermal process. *Inorganic Chemistry*, *47*, 7071–7073.

How to cite this article: Pandey PC, Pandey G, Narayan RJ. Microneedle-based transdermal electrochemical biosensors based on Prussian blue-gold nanohybrid modified screen-printed electrodes. *J Biomed Mater Res*. 2020;1–17. https://doi.org/10.1002/jbm.b.34678